INTERNATIONAL JOURNAL FOR NUMERICAL METHODS IN FLUIDS, VOL. 6, 927–937 (1986)

COMPUTATION OF INTERNAL TURBULENT FLOW WITH A LARGE SEPARATED FLOW REGION

UPENDER K. KAUL* AND DOCHAN KWAK†

NASA Ames Research Center, Moffett Field, California 94035, U.S.A.

SUMMARY

An implicit two-equation turbulence solver, KEM, in generalized co-ordinates, is used in conjunction with the three-dimensional incompressible Navier–Stokes solver, INS3D, to calculate the internal flow in a channel and a channel with a sudden 2:3 expansion. A new and consistent boundary procedure for a low Reynolds number form of the k–ε turbulence model is chosen to integrate the equations up to the wall. The high Reynolds number form of the equations is integrated using wall functions. The latter approach yields a faster convergence to the steady-state solution than the former. For the case of channel flow, both the wall-function and wall-boundary-condition approaches yield results in good agreement with the experimental data. The back-step (sudden expansion) flow is calculated using the wall-function approach. The predictions are in reasonable agreement with the experimental data.

KEY WORDS Two-equation Turbulence Model Separated Flow

INTRODUCTION

The need for a general three-dimensional (3-D) turbulent flow solver in generalized co-ordinates is growing as the computing power of the supercomputers increases. Until now, either for simplicity or for computing limitations, or for both, some approximations were necessary to reduce the complexity of the Reynolds-averaged Navier–Stokes equations so that a flow colud be simulated in a reasonable time and at a reasonable expense. Therefore, thin-layer, or the parabolized Navier–Stokes equations, have been widely used wherever applicable. With improved resources it is now possible to calculate the 3-D internal turbulent flows in which the thin layer or parabolization approximation may break down.

The need for such a general, turbulent flow solver has been emphasized by the Space Shuttle main engine (SSME) redesign and development work. The 3-D incompressible Navier–Stokes code, INS3D, developed by Kwak *et al.*,[1] has been used to compute various laminar flows,[2–7] with particular reference to the SSME redesign process. The INS3D code, based on the artificial compressibility method of Chorin,[8] has been evolved from the two-dimensional and axisymmetric solvers of Steger and Kutler,[9] and Chakravarthy,[10] respectively. In the present work, an implicit, two-equation, k–ε turbulence solver, KEM, developed by Kaul,[11] is used in conjunction with INS3D to calculate internal flows in a channel, and a channel with a 2:3 sudden expansion. The latter corresponds to internal flow over a backward-facing step. The present k–ε turbulence solver, which solves the 3-D transport equations for the turbulent kinetic energy, k, and its dissipation

* Principal Analyst, Sterling Software, Palo Alto, CA, U.S.A.; Member, AIAA
† Research Scientist; Member, AIAA.

0271-2091/86/120927-11$05.50

Received 15 August 1985
Revised 15 May 1986

rate, ε, in generalized co-ordinates, with the diffusion terms retained in all the three directions, can be used in conjunction with compressible or incompressible flow solvers to compute the turbulent flows of interest.

The channel flow was selected to quantitatively assess effectiveness of the wall-function and wall-boundary-condition approaches, using high and low Reynolds number formulations, respectively, and to test the new and consistent boundary procedure for the low Reynolds number formulation used in this study.

The flow over a backward-facing step is one of the simpler separated flows because the location of the separation point is predetermined from geometric considerations rather than from pressure-gradient considerations. However, because the location of the reattachment point is very sensitive to the pressure gradient, its prediction is an excellent test for the validity of the turbulence model used. The separated region between these two points extends about seven step heights, with some uncertainty caused by the ambiguity in the location of the reattachment point. This region exhibits a strong streamwise pressure gradient. However, the transverse pressure gradient is small. Because of the latter, it is possible to do momentum integral analysis[12] across the flow with some empirical input to calculate the turbulent velocity profiles based on a mixing-length hypothesis. Although k–l turbulence models have been used to predict the turbulent flow over surface obstructions,[12,13] the k–ε models tend to yield better predictions, especially for internal flows. This is partly due to the fact that the boundary conditions on the length scale, l, are difficult to prescribe realistically.

The flow over the back-step has many other features associated with it that make it a very attractive problem to study both experimentally and computationally. The flow at the separation point has a boundary-layer profile of an oncoming flow. When the flow detaches, a shear layer grows downstream just as in a free jet boundary. In this region, vortices roll up and coalesce with one another, thus thickening the shear layer. This mechanism is the same as that found in a free-shear layer. But for the step-side wall, this process of coalescence would continue downstream. However, because of the presence of the step-side wall, the flow experiences a drastic change. The lower edge of the shear layer, as it approaches the wall, experiences a streamwise deceleration and an increase in pressure, thereby an adverse streamwise pressure gradient is set up. Because of this adverse pressure gradient, flow reversal eventually takes place, and in this process the reattachment point is formed. This sets up the recirculating flow in the separation bubble thus formed. The lower edge of the shear layer grows linearly downstream from the base of the step as it would in a free-shear layer. Only near the reattachment point does it get distorted and curve sharply toward the wall. This edge of the shear layer is therefore called the dividing streamline. The recirculation region is maintained by the flow reversal near the reattachment point, and the entrainment along the dividing streamline into the shear layer.

TURBULENCE MODEL

By using Einstein's index notation and the summation convention, transport equations for k and ε can be written in Cartesian co-ordinates as the following 2×2 system:

$$\partial_t D + (\mathbf{F}_i - \mathbf{F}_{v_i})_{,i} = \mathbf{S},$$

with the turbulence kinetic energy and the homogeneous dissipation rate, respectively, given by

$$k = \frac{1}{2}\overline{u_i u_i} \text{ and } \varepsilon = \left(\frac{\mu}{\rho}\right)\overline{u_{i,j} u_{i,j}},$$

where the solution vector is

$$\mathbf{D} = \begin{bmatrix} \rho k \\ \rho \varepsilon \end{bmatrix},$$

the flux vectors are

$$\mathbf{F}_i = \begin{bmatrix} \rho U_i k \\ \rho U_i \varepsilon \end{bmatrix} \text{ and } \mathbf{F}_{v_i} = \frac{1}{Re_\infty} \begin{bmatrix} \mu_k k_{,i} \\ \mu_\varepsilon \varepsilon_{,i} \end{bmatrix},$$

and the source term is

$$\mathbf{S} = \frac{1}{Re_\infty} \begin{bmatrix} P - \rho \varepsilon Re_\infty - 2\mu \dfrac{k}{d^2} \\ C_1 \dfrac{\varepsilon}{k} P - C_2 f_2 \dfrac{\rho \varepsilon^2}{k} Re_\infty - \dfrac{2\mu\varepsilon}{d^2} f_3 \end{bmatrix}.$$

The kinetic energy production term due to the mean shear is given by

$$P = -\rho \overline{u_i u_j} U_{i,j},$$

where U_i is the mean velocity and u_i is the fluctuating velocity. On application of the gradient diffusion hypothesis (Boussinesq, 1877), the production term can be written as

$$\left[\mu_t (U_{i,j} + U_{j,i}) - \frac{2}{3} \rho k \delta_{ij} \right] U_{i,j},$$

where δ_{ij} is the Kronecker delta, and the turbulent viscosity μ_t is given by Kolmogorov's hypothesis,[14]

$$\mu_t = C'_\mu \rho k^{1/2} l Re_\infty.$$

Since at high Reynolds numbers the dissipation rate, ε, can be assumed to be proportional to $k^{3/2}/l$, we can write

$$\mu_t = \frac{C_\mu \rho k^2}{\varepsilon} Re_\infty,$$

where C_μ and C'_μ are constants. Also $\mu_k = \mu + (\mu_t/\sigma_k)$, and $\mu_\varepsilon = \mu + (\mu_t/\sigma_\varepsilon)$, where μ_t/σ_k and μ_t/σ_ε play the roles of effective exchange or diffusion coefficients for k and ε, respectively, and where σ_k and σ_ε can be interpreted as turbulent Prandtl numbers for the k and ε transport processes. Hence, σ_k and σ_ε can be assumed to be close to unity in accordance with expectations. The turbulent viscosity is redefined as

$$\mu_t = C_\mu f_\mu \frac{\rho k^2}{\varepsilon} Re_\infty$$

The functions f_2 and f_μ above take into account the low Reynolds number dependence of the constants,[15,16] C_2 and C_μ, and they are defined as

$$f_2 = [1{\cdot}0 - \exp(-R_T^2)],$$

$$f_\mu = \exp\left[\frac{-3{\cdot}4}{\left(1{\cdot}0 + \dfrac{1}{50} R_T\right)^2} \right].$$

The terms $-(2\mu k/d^2)$ in the k equation and $-[(2\mu\varepsilon/d^2)f_3]$ in the ε equation take into account the low Reynolds number effect near the walls and are discussed in Reference 17. The function f_3 is given by

$$f_3 = \exp\left[-C_3\left(\frac{\rho V_\tau d}{\mu} Re_\infty\right)\right],$$

where V_τ is the friction velocity, and d is the normal distance to the wall. The high Reynolds number values of the various 'constants' are chosen as

$$\sigma_\varepsilon = 1{\cdot}3, \qquad C_2 = 2{\cdot}0,$$
$$\sigma_k = 1{\cdot}0, \qquad C_3 = 0{\cdot}5,$$
$$C_1 = 1{\cdot}44, \qquad C_\mu = 0{\cdot}09.$$

The coefficient of viscosity μ is normalized by μ_∞, velocities are normalized by U_∞, distances by a characteristic length L, and the density ρ by ρ_∞. This results in the reference Reynolds number definition as

$$Re_\infty = \frac{\rho_\infty U_\infty L}{\mu_\infty}.$$

The turbulent kinetic energy k is normalized by U_∞^2 and the dissipation rate ε is normalized by U_∞^3/L.

Although an exact equation for the dissipation rate, ε, can be derived from the instantaneous form of the Navier–Stokes equations,[18] the transport equation for ε used here is based on heuristic grounds[19] since the exact equation requires drastic model assumptions that yield an ε equation with highly empirical character. The equations for k and ε used here are applicable for both high and low values of the turbulent Reynolds number

$$R_T = \frac{\rho k^2}{\mu\varepsilon} Re_\infty.$$

Near the wall, the high Reynolds number form of the k–ε system is modified as follows. The viscous diffusion of k and ε is included in the governing equations. The constants C_2 and C_μ are allowed to be functions of the turbulent Reynolds number, R_T, and appropriate terms are added to the high Reynolds number form of the k–ε equation.[15–17] Since the total dissipation rate is not zero at the wall and the isotropic dissipation there vanishes, a term for the dissipation at the wall is chosen which corresponds to the non-isotropic part of the energy dissipation. Accordingly, the term $-2\mu k/d^2$ is added to the right hand side of the k equation.[17] With both the high and low Reynolds number forms thus built into the k–ε system, the governing equations can be solved subject to the boundary conditions applied either at the wall or away from the wall through the use of wall functions.[20]

BOUNDARY CONDITIONS

In the present study, the boundary procedure for the low Reynolds number formulation is made consistent by setting the dissipation rate at the wall equal to its non-isotropic value, $2\mu k_P/d_P^2$, where the subscript P refers to the point next to the wall. This eliminates the need for adding the 'wall dissipation' term $-2(\mu\varepsilon/d^2)f_3$, which involves an additional constant C_3.[17] Also the term $-2\mu k/d^2$ is removed from the governing equation for k. This procedure is seen to be well behaved, and yields

predictions in good agreement with experimental data. Alternatively, the zero-gradient condition on ε at the wall is employed, with the term $-2\mu k/d^2$ retained in the k equation. Both the wall-flux and the wall zero-gradient boundary condition on ε yield accurate predictions for a channel flow. Of course, the turbulent kinetic energy at the wall is set equal to zero. A more accurate boundary condition on ε, given in Reference 21, is used, and is valid very close to the wall for approximately $y^+ \leqslant 0{\cdot}6$. This condition is given by

$$\varepsilon_w = \frac{4\mu k}{d^2} - \varepsilon_P,$$

where subscripts w and P refer to the wall and the next point off the wall, respectively. It is interesting to note that in situations in which the zero-gradient condition is satisfied, all of the three previous conditions become identical. The predictions for channel flow using this condition are essentially the same as those given by the earlier boundary conditions.

For the case of high Reynolds number formulation, a wall-function approach is adopted which precludes having to integrate right down to the walls. The wall-function approach[20] is used to connect the outer region to the viscous sublayer. The assumption here is that the resultant tangential velocity at a point P near the wall outside the viscous sublayer follows the logarithmic law of the wall, and the turbulence is in local equilibrium at such a point, i.e. the rate of production of the turbulence kinetic energy equals the rate at which it is dissipated. Then, at such a point, P, we have

$$\frac{V_P}{V_\tau} = \frac{1}{\kappa} \ln \left[E \frac{\rho V_\tau d_P}{\mu} Re_\infty \right],$$

where E is a parameter which accounts for surface roughness, friction, or phenomena such as pressure gradient or mass injection through the walls; κ is the von Karman constant ($= 0{\cdot}42$), V_P is the resultant tangential velocity at P, V_τ is the resultant friction velocity and is equal to $\sqrt{(\tau_w/\rho)}$, and d_P is the normal distance between P and the wall. The kinetic energy and the dissipation rate at P are then given by

$$k_P = \frac{V_\tau^2}{\sqrt{C_\mu}} \quad \text{and} \quad \varepsilon_P = \frac{V_\tau^3}{\kappa d_P}.$$

Dirichlet inflow conditions and Neumann outflow and far-field conditions in external flows are used to complete the necessary boundary-condition procedure.

The numerical scheme used to integrate the k–ε system in generalized coordinates is the implicit non-iterative approximate factorization algorithm of Beam and Warming.[22] The reader is referred to Reference 11 for details.

RESULTS AND DISCUSSION

The k–ε turbulence model was used to compute the flow in a channel and a channel with a 2:3 sudden expansion. The latter represents an internal flow over a backward-facing step. The computational mesh used was a two-dimensional Cartesian grid system which was stretched in streamwise and cross-flow directions. For the case of channel calculations, 91 grid points were used in the cross-flow direction and 101 points were used in the streamwise direction. For the back-step calculations, an 85×141 (cross-flow and streamwise directions, respectively) grid was used. The k–ε solver, KEM, was made to lag the INS3D flow solver by one time step. To test the convergence property of the turbulent flow solver, a known, fully developed turbulent-channel velocity profile was imposed and the k–ε solver was iterated to produce a converged solution of the k–ε system

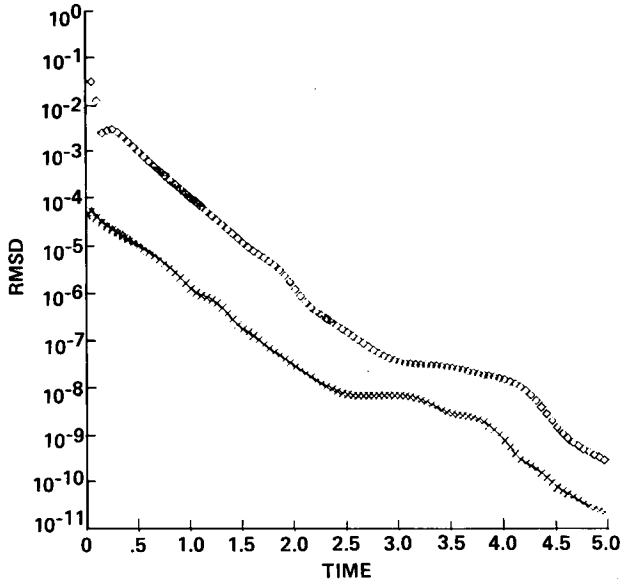

Figure 1. A comparison of the solution convergence history corresponding to the present wall-boundary-condition and the wall-function approaches: ◇ wall-flux B.C.; × wall function

by switching off the INS3D. The convergence history is shown in Figure 1, in which the root-mean-square values (RMSD) of the change in the solution vector from one time step to another are plotted against the normalized time τ. A comparison was made between the wall-flux boundary condition and the wall-function approach. The wall-function approach exhibits superior convergence characteristics. However, both wall-flux boundary condition and wall-function approaches yield a very fast convergence on the k–ε solution, as is shown by the RMSD plots.

The channel flow was simulated at a Reynolds number of 27,600 based on the channel half-width. Both high and low Reynolds number forms of the k–ε model were solved. The low Reynolds number form was calculated using the present wall-flux, zero-gradient ε boundary conditions and Chien's formulation.[17] The wall-flux and zero-gradient boundary conditions on ε yield almost identical results. A comparison of the plots of k/V_τ^2 versus y^+ corresponding to the three boundary procedures and the experiments of Clark[23] is shown in Figure 2. The comparison shows a generally good agreement, except near the walls, where the experimental data are underpredicted by all three computational results. The wall-flux boundary condition yields a slightly better agreement with the experiments. High Reynolds number calculations with wall functions that were used here give a good overall agreement with the experiments, although they tend to underpredict the experiment in general.

The flow over a backward-facing step was simulated using wall functions. The calculations correspond to Reynolds number, $Re = 44{,}580$, based on the step height, h. The experimental data used for comparison are those of Kim *et al.*[24] The computational results of Mansour *et al.*[25] were also used for an added comparison. The present calculations yield a separation length of 5·2 h, which is approximately the same as that in Reference 25. However, by incorporating the effects of curvature by introducing a rotation rate term in the ε equation, the reattachment point was located at 6·6 h in Reference 25. The effect of the curvature term is to account for the sharp curvature of the dividing streamline near the reattachment point, and thus to modify the location of this point. In

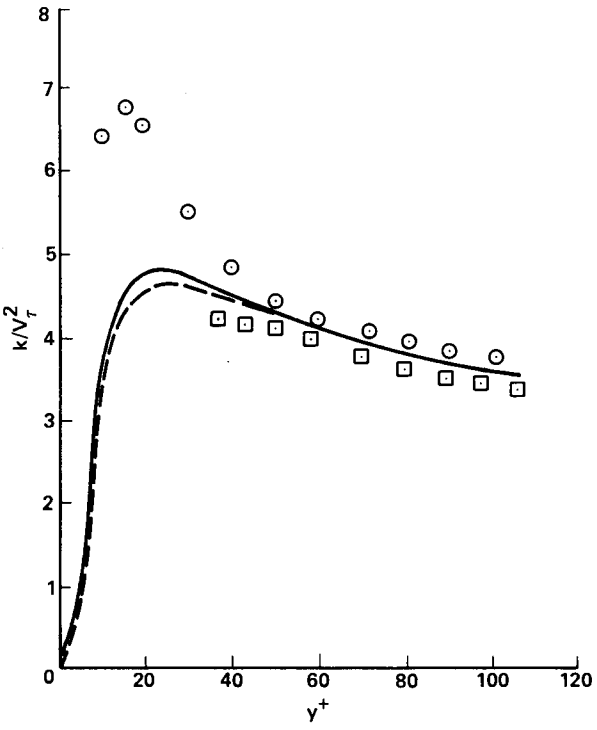

Figure 2. Variation of the turbulence kinetic energy, k with y^+ showing its near wall behaviour for channel flow: ○ experiment;[23] □ computation—wall function; ——— computation;[17] ——— computation—wall B.C.

the present calculations, no attempt was made to introduce any effects of curvature of streamlines either through the ε equation, or through the defining equation for μ_t. Figure 3 is a plot of the mean velocity profile at the reattachment point as predicted by the present computations and those of Reference 25. The agreement between the profiles from the two computations is good. However, since the reattachment point is seen to be located at about 7 h in the experiment,[24] with some uncertainty, the comparison of the two computations with the experiment is not favourable. In Figure 4, the mean velocity profiles are plotted at $x/h = 10{\cdot}7$, which is downstream of the reattachment point. The agreement among the two computations and the experiment at this location is good.

The turbulence kinetic energy, k, profiles at $x/h = 7{\cdot}7$ are shown in Figure 5. Away from the wall, present computations overpredict the experiments. This can be construed as the reason that the reattachment length is underpredicted in the present computations. Since the eddies in the shear layer coalesce downstream of the base of the step, the length scale of the turbulence carrying eddies increases. It is this length scale that is overpredicted by the present computations, therefore resulting in a rapid growth rate of the shear layer, and thus resulting in a premature reattachment at $5{\cdot}2h$. Since the corresponding computational results of Reference 25 take the curvature effects into account, these results underpredict k given by the present computations; however, they also underpredict k given by the experiment.[24] The reason for this is that the experiments also have an uncertainty in the prediction of the reattachment point, by over a step height, which could place the reattachment point at less than 6 step heights away from the base. Figure 6 shows the turbulent shear stress distribution at $x/h = 7{\cdot}7$. Again, the same behaviour is exhibited by the computations

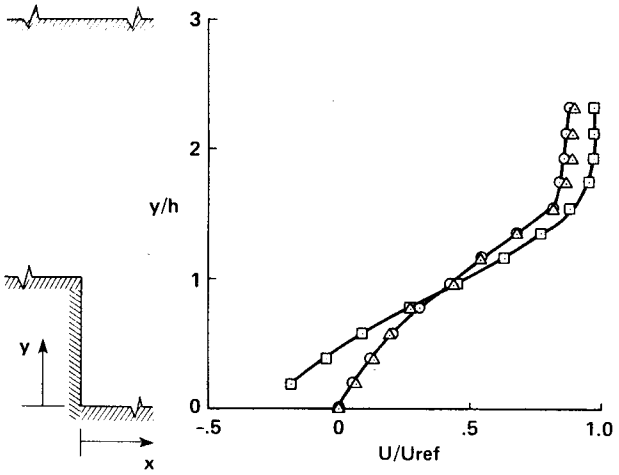

Figure 3. A comparison of the mean velocity profiles at the computed reattachment point, $x = 5{\cdot}2\,h$, for the backward-facing step flow: □ experiment;[24] ○ present computation; △ computation[25]

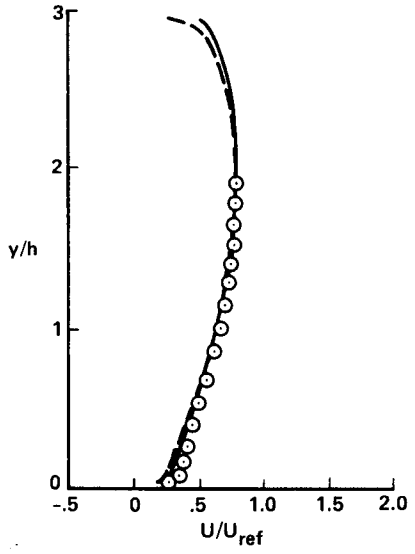

Figure 4. A comparison of the mean velocity profiles at $x = 10{\cdot}7h$: ○ experiment;[24] ——— present computation; —— computation[25]

as in the turbulent kinetic energy plot in Figure 5, thus reinforcing the conclusion that it is this overprediction mechanism in the k–ε system that is responsible for the reattachment point location being underpredicted. Although the peak as given by the experiment[24] is not matched by the computations in Figure 6, the discrepancy is not as much as in the k comparison in Figure 5. That the discrepancies between the experimental data and the predictions are due to the overprediction mechanism in the k–ε system has been alluded to by various authors, e.g. Hackman *et al.*[26] point out this particular deficiency of the k–ε system. They also point out that the upwind differencing schemes are inadequate for step flows. However, the numerical algorithm used here is based on the central-difference approximation of the spatial derivatives, which entails some form of

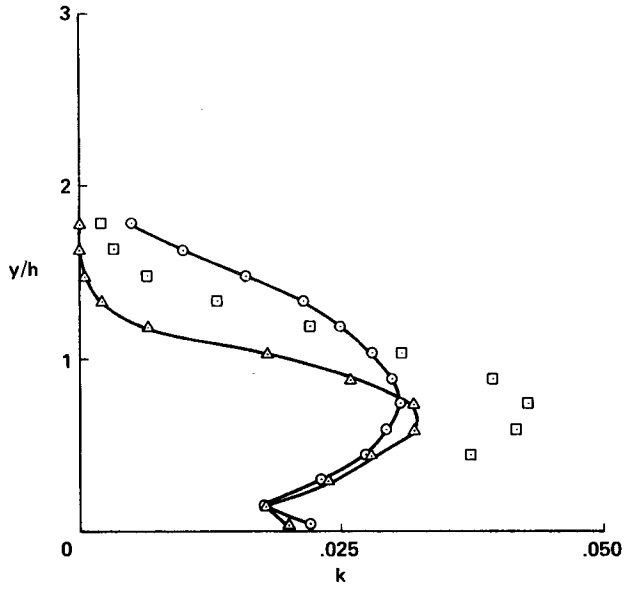

Figure 5. Variation of the turbulence kinetic energy, k, in the cross-flow direction at $x = 7{\cdot}7\,h$: □ experiment;[24] ○ present computation; △ computation[25]

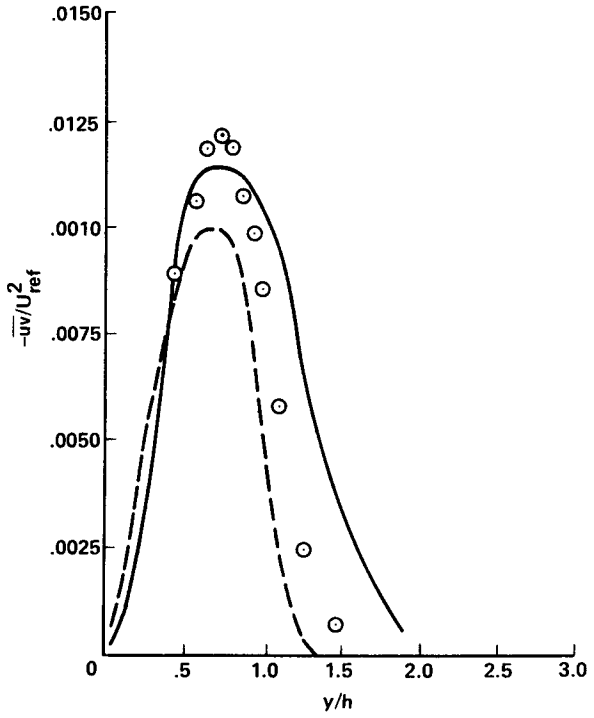

Figure 6. Turbulent shear-stress distribution in the cross-flow direction at $x = 7{\cdot}7\,h$: ○ experiment;[24] ——— computation;[25] ——— computation—wall function

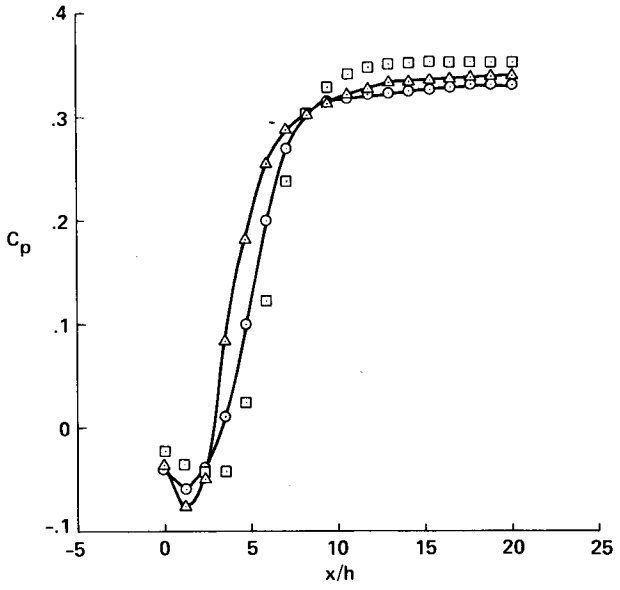

Figure 7. A comparison of pressure distributions on the step-side wall: □ experiment;[24] ○ present computation; △ computation[25]

smoothing to damp out the high frequency errors that arise from this approximation. The importance of the interaction of these smoothing parameters with the grid systems, and the numerical algorithms used, has been discussed in Reference 27. In view of this discussion, and the fact that the computational grid used here is sufficiently fine to have achieved a grid-independent solution, any discrepancies between the predictions and the experimental data are expected to be mainly due to the inadequacies in the turbulence model.

Finally, the pressure distribution on the step-side wall is shown in Figure 7. The pressure coefficient, given by

$$C_P = \frac{p - p_{ref}}{(1/2)\rho U_{ref}^2},$$

is plotted against the downstream distance x/h. Pressure prediction directly beneath the separation point on the step-side wall is not as good as that downstream. The pressure minimum as given computationally shows a sharper profile around it than that given by the experiment. This is directly related to the fact that the computations do not adequately predict the flow phenomenon in the corner between the step base and the step-side wall. The agreement between the present computation and the computations of Reference 25 is good. Both computations underpredict the experiment downstream of the reattachment point.

CONCLUDING REMARKS

Turbulent channel and backward-facing step flows have been simulated using a k–ε model of turbulence. A new and consistent wall boundary procedure has been employed in this study for a low Reynolds number formulation. This procedure makes the k–ε solver robust, and it yields predictions in somewhat better agreement with the experimental data for a channel flow than other formulations. Both wall-function and wall-boundary-condition approaches yield results in good agreement with the experimental data for the case of a channel flow. For the case of a back-step, the wall-function approach used in this study yields results in a favourable comparison with the experiment. However, the predictions are in good agreement with the experiment downstream of

the reattachment point. Calculations were performed on the CRAY/XMP-12. The computational time per grid point per time step with the partially vectorized code was $0{\cdot}18 \times 10^{-3}$s. The storage requirement for the back-step problem was approximately 270,000 decimal words.

ACKNOWLEDGEMENT

This work was sponsored by NASA Marshall Space Flight Center.

REFERENCES

1. D. Kwak, J. L. C. Chang, S. P. Shanks and S. R. Chakravarthy, 'An incompressible Navier–Stokes flow solver in three-dimensional curvilinear coordinate system using primitive variables', *AIAA Paper 84-0253, AIAA 22nd Aerospace Sciences Meeting*, Reno, Nevada, 1984; also, *AIAA J.*, **24,** 390–396 (1986).
2. J. L. C. Chang and D. Kwak, 'On the method of pseudocompressibility for numerically solving incompressible flow', *AIAA Paper 84-0252*, Reno, Nevada, 1984.
3. D. Kwak, J. L. C. Chang and S. P. Shanks, 'A solution procedure for three-dimensional incompressible Navier–Stokes equations and its application', *Ninth International Conference on Numerical Methods in Fluid Dynamics*, C.E.N. Saclay, France, 1984.
4. U. K. Kaul, D. Kwak and C. Wagner, 'A computational study of saddle point separation and horseshoe vortex system', *AIAA Paper 85-0182, AIAA 23rd Aerospace Sciences Meeting*, Reno, Nevada, 1985.
5. J. L. C. Chang, D. Kwak and S. C. Dao, 'A three-dimensional incompressible flow simulation method and its application to the space shuttle main engine, part 1: laminar flow', *AIAA Paper 85-0175*, Reno, Nevada 1985.
6. S. E. Rogers, D. Kwak and U. K. Kaul, 'On the accuracy of the pseudo-compressibility method in solving the incompressible Navier–Stokes equations', *AIAA Paper 85-1689*, Cincinnati, Ohio, 1985.
7. S. E. Rogers, D. Kwak and U. K. Kaul, 'A numerical study of three-dimensional incompressible flow around multiple posts', *AIAA Paper 86-0353*, Reno, Nevada 1986.
8. A. J. Chorin, 'A numerical method for solving incompressible viscous flow problems', *J. Computational Physics*, **2,** 12–26 (1967).
9. J. L. Steger and P. Kutler, 'Implicit finite-difference procedures for the computation of vortex wakes', *AIAA J.*, **15,** 581–590 (1977).
10. S. R. Chakravarthy, 'Numerical simulation of laminar incompressible flow within liquid filled shells', *Report ARBRL-CR-00491*, U.S. Army Ballistics Research Laboratory, Aberdeen Proving Ground, Md., 1982.
11. U. K. Kaul, 'An implicit finite-difference code for a two-equation turbulence model in three-dimensional coordinates', *NASA TM-86752*, 1985.
12. U. K. Kaul and W. Frost, 'Turbulent atmospheric flow over a backward facing step', *NASA CR-2749*, 1976.
13. W. Frost, J. Bitte, and C. F. Shieh, 'Analysis of neutrally stable atmospheric flow over a two-dimensional forward facing step', *AIAA J.*, **18,** 32–38 (1980).
14. A. M. Kolmogorov, 'Equations of turbulent motion of an incompressible turbulent fluid', *Izvestia Akademii Nauk Uzbekskoi SSR Series Phys. VI*, No. 1–2, 56–58 (1942); translated into English at Imperial College, Mechanical Engineering Dept., *Rept. ON/6* (1968).
15. W. P. Jones and B. E. Launder, 'The calculation of low Reynolds number phenomena with a two-equation model of turbulence', *Int. J. Heat Mass Transfer*, **16,** 1119–1130 (1973).
16. W. P. Jones and B. E. Launder, 'The prediction of laminarization with a two-equation model of turbulence', *Int. J. Heat Mass Transfer*, **15,** 301–314 (1972).
17. K. Y. Chien, 'Predictions of channel and boundary-layer flows with a low Reynolds number model', *AIAA J.*, **20** (1982).
18. F. H. Harlow and P. I. Nakayama, 'Transport of turbulent energy decay rate', *Los Alamos Sci Lab Report LA-3854*, 1968.
19. K. Hanjalic, 'Two-dimensional asymmetrical turbulent flow in ducts', *Ph. D. Thesis*, University of London, 1970.
20. W. Rodi, 'Examples of turbulence models for incompressible flows', *AIAA J.*, **20,** 872–879 (1982).
21. D. R. Chapman and G. D. Kuhn, 'Navier–Stokes computations of viscous sublayer flow and the limiting behavior of turbulence near a wall', *AIAA Paper 85-1487, AIAA 7th Computational Fluid Dynamics Conference*, Cincinnati, Ohio, 1985.
22. R. M. Beam and R. F. Warming, 'An implicit factored scheme for the compressible Navier–Stokes equations', *AIAA J.*, **16,** 393–402 (1978).
23. J. A. Clark, 'A study of incompressible turbulent boundary layers in channel flow', *J. Basic Eng.*, **90** (1968).
24. J. Kim, S. J. Kline and J. P. Johnston, 'Investigation of a reattaching turbulent shear layer: flow over a backward-facing step', *J. Fluids Engineering, ASME Trans.*, **102,** 302 (1980).
25. N. N. Mansour, J. Kim and P. Moin, 'Computation of turbulent flows over a backward-facing step', *NASA TM 85851*, 1983.
26. L. P. Hackman, G. D. Raithby and A. B. Strong, 'Numerical predictions of flows over backward-facing steps', *Int. j. numer. methods fluids*, **4,** 711–724 (1984).
27. U. K. Kaul and D. S. Chaussee, 'A comparative study of the parabolized Navier–Stokes code using various grid-generation techniques', *Computers and Fluids*, **13,** 421–441 (1985).